Proc. of the European Safety and Reliability Conference (ESREL 2026)
Edited by José C. Matos, Paulo B. Lourenço, Michael Beer, Daniel Oliveira, Edoardo Patelli, Hélder S. Sousa, Rui A. Silva and Monica Santamaria

doi: 10.3850/ESREL2026061419_esrel26-p26108-cd

Convex Optimization Framework for Probabilistic Inverse Problem Identification Based on the Principle of Probability Preservation

Yuhan Zhu

College of Civil Engineering, Tongji University, China. E-mail: 2310475@tongji.edu.cn

Jie Li

State Key Laboratory of Disaster Reduction in Civil Engineering, Tongji University, China.
E-mail: lijie@tongji.edu.cn

This paper investigates the probabilistic inverse problem in physical stochastic systems, which seeks to infer the underlying probability structure of an unobservable random source based on observed system responses. Grounded in the Principle of Preservation of Probability, a unified convex optimization framework is proposed that requires minimal prior assumptions. The core approach discretizes the random source space into subdomains, transforming the identification task into a quadratic programming problem with linear constraints to determine the probability measure assigned to each subdomain. Two complementary implementations are introduced. The first directly utilizes the transient probability density function (PDF) of the system response. The second, termed the Diffusion Manifold Method, operates directly on raw response data by projecting it onto an intrinsic Riemannian manifold, enabling effective handling of high-dimensional outputs and measurement noise. A singular value decomposition (SVD) of the resulting system transition probability matrix provides a criterion for well-posedness, revealing that solvability depends on the injectivity of the system mapping. In cases where the problem is ill-posed, the PDF of the random source is reconstructed as a linear combination of eigenmodes. A two-step optimization procedure is then applied: first, the identifiable eigenmodes of the source PDF are recovered from the response; second, the unidentifiable modes are regularized using quality metrics, such as maximum entropy. Numerical examples demonstrate that the proposed methods reliably recover complex and irregular probability structures, including joint distributions, even in the presence of noise and with limited data—without relying on strong prior assumptions.

Keywords: Probabilistic Inverse Problem, Principle of Preservation of Probability, Convex Optimization, Ill-posed Problem, Riemannian Manifold.

1. Background and Introduction

In physical stochastic systems, identifying the probability structure of unobservable random sources from observed responses—known as the probabilistic inverse problem—is essential for uncertainty quantification. Two main approaches have been developed: Bayesian inference and optimization-based methods Ye et al. (2019).

Under the Bayesian framework, solving the probabilistic inverse problem typically relies on sampling-based inference, with Markov Chain Monte Carlo (MCMC) methods serving as a foundational tool Geman and Geman (1984); Gelfand and Smith (1990). To enhance computational efficiency in high-dimensional settings, advanced variants such as Hamiltonian Monte Carlo Nagel and Sudret (2016) and transitional MCMC Lye et al. (2022); Wu et al. (2025) have been developed. These are increasingly integrated with techniques like variational inference Cabral et al. (2024); Mo and Yan (2025) and manifold learning Chen et al. (2022); Berenfeld et al. (2024), the latter of which projects the posterior distribution onto a low-dimensional Riemannian submanifold embedded in the response space, thereby mitigating the curse of dimensionality and sharp-peaked likelihood issues.

On the other hand, optimization-based approaches reformulate the inverse problem as a deterministic minimization task. This typically involves selecting an appropriate objective function, such as the likelihood or a statistical distance like f-divergence Liese and Vajda (2006) or the Wasserstein metric Peyré et al. (2019); Feydy et al. (2019). These approaches often incorporate regularization terms to ensure convexity and numerical well-posedness.

The study of probabilistic inverse problems presents a unified but fragmented landscape, focusing on inferring source distributions but with diverse theories and methods across disciplines.

This paper introduces a convex optimization framework based on the principle of preservation of probability. The method transforms identifying the random source into a quadratic programming problem, requiring no prior distributional assumptions. A singular value decomposition (SVD) criterion assesses well-posedness, with regularization for non-injective cases. Two approaches are offered: one using the response probability density function (PDF) Zhu and Li (2025b), and the Diffusion Manifold Method Zhu and Li (2025a), which utilizes the low-dimensional manifold structure of response data to manage high-dimensional outputs and noise.

2. The Identification Method Based on Density

Consider a physical stochastic system governed by the following operator equation:

$$\mathcal{L}(\boldsymbol{U}, \boldsymbol{\Theta}, t) = 0 \tag{1}$$

where $\mathcal{L}$ is any differential, integral, or algebraic operator; $\boldsymbol{U} \in \Omega_{\boldsymbol{U}}$ is the system response time history; $\Omega_{\boldsymbol{U}} \subseteq \mathbb{R}^{d_{\boldsymbol{U}}}$ is the value space of $\boldsymbol{U}$; $\boldsymbol{\Theta} \in \Omega_{\boldsymbol{\Theta}} \subseteq \mathbb{R}^{d_{\boldsymbol{\Theta}}}$ is the random source, essentially a finite-dimensional random vector; $\Omega_{\boldsymbol{\Theta}}$ is the random source space where $\boldsymbol{\Theta}$ takes values. Li and Chen (2008)

Based on the principle of preservation of probability, the probability density evolution theory demonstrates that the joint PDF of $\boldsymbol{U}, \boldsymbol{\Theta}$ is governed by the generalized density evolution equation (GDEE) Li and Chen (2008), with the following initial and natural boundary conditions satisfied:

$$\frac{\partial p_{\boldsymbol{U}\boldsymbol{\Theta}}(\boldsymbol{u}, \boldsymbol{\theta}, t)}{\partial t} + \sum_i U_i(\boldsymbol{\theta}, t) \frac{\partial p_{\boldsymbol{U}\boldsymbol{\Theta}}(\boldsymbol{u}, \boldsymbol{\theta}, t)}{\partial u_i} = 0 \tag{2a}$$

$$p_{\boldsymbol{U}\boldsymbol{\Theta}}(\boldsymbol{u}, \boldsymbol{\theta}, 0) = \boldsymbol{\delta}(\boldsymbol{u} - \boldsymbol{u}_0) p_{\boldsymbol{\Theta}}(\boldsymbol{\theta}) \tag{2b}$$

$$\lim_{\|\boldsymbol{u}\| \to \infty} p_{\boldsymbol{U}\boldsymbol{\Theta}}(\boldsymbol{u}, \boldsymbol{\theta}, t) = 0 \tag{2c}$$

where U_i is the i-th component of $\boldsymbol{U}$; $U_i(\boldsymbol{\theta}, t)$ represents the formal solution of U_i given $\boldsymbol{\Theta} = \boldsymbol{\theta}$; $\boldsymbol{\delta}(\bullet)$ stands for the multi-dimensional generalized Dirac function; $\boldsymbol{u}_0$ is the initial value of the system; and $p_{\boldsymbol{\Theta}}(\boldsymbol{\theta})$ denotes the PDF of $\boldsymbol{\Theta}$. The solution of Eq. (2a) can be written in the following form:

$$p_{\boldsymbol{U}\boldsymbol{\Theta}}(\boldsymbol{u}, \boldsymbol{\theta}, t) = \boldsymbol{\delta}[\boldsymbol{u} - \boldsymbol{U}(\boldsymbol{\theta}, t)] p_{\boldsymbol{\Theta}}(\boldsymbol{\theta}) \tag{3}$$

where $\boldsymbol{U}(\boldsymbol{\theta}, t)$ represents the formal solution of $\boldsymbol{U}$ conditioned on $\boldsymbol{\Theta} = \boldsymbol{\theta}$. The PDF of the response $\boldsymbol{U}$ can be calculated by the following integral:

$$p_{\boldsymbol{U}}(\boldsymbol{u}, t) = \int_{\Omega_{\boldsymbol{\Theta}}} p_{\boldsymbol{U}\boldsymbol{\Theta}}(\boldsymbol{u}, \boldsymbol{\theta}, t) \mathrm{d}\boldsymbol{\theta} \tag{4}$$

In this section, the PDF $p_{\boldsymbol{\Theta}}(\boldsymbol{\theta})$ is inferred from the observation of $p_{\boldsymbol{U}}(\boldsymbol{u}, t)$ at multiple time instants $\{t_i\}_{i=1}^{N_t}$. First, a set of uniformly distributed points $\mathcal{P}_{\text{par}} = \{\boldsymbol{\theta}_q\}_{q=1}^{N_{\text{par}}} \subseteq \Omega_{\boldsymbol{\Theta}}$ is selected, with $\Omega_{\boldsymbol{\Theta}}$ partitioned into Voronoi cells. For any $q = 1, 2, ..., N_{\text{par}}$, the Voronoi cell Ω_q associated with $\boldsymbol{\theta}_q \in \mathcal{P}_{\text{par}}$ is defined as:

$$\Omega_q = \{\boldsymbol{\theta} \in \Omega_{\boldsymbol{\Theta}} : \|\boldsymbol{\theta} - \boldsymbol{\theta}_q\| \leq \|\boldsymbol{\theta} - \boldsymbol{\theta}_l\|, \forall \boldsymbol{\theta}_l \in \mathcal{P}_{\text{par}}\} \tag{5}$$

The identification of $p_{\boldsymbol{\Theta}}$ can be transferred into identifying the probability measure $\mathrm{Pr}_q = \mathrm{Pr}_{\boldsymbol{\Theta}}(\Omega_q)$ of each cell. The integral in Eq. (4) can be discretized via the partition of $\Omega_{\boldsymbol{\Theta}}$:

$$\begin{aligned} p_{\boldsymbol{U}}(\boldsymbol{u}, t) &= \sum_{q=1}^{N_{\text{par}}} \int_{\Omega_q} \boldsymbol{\delta}[\boldsymbol{u} - \boldsymbol{U}(\boldsymbol{\theta}, t)] p_{\boldsymbol{\Theta}}(\boldsymbol{\theta}) \mathrm{d}\boldsymbol{\theta} \\ &\approx \sum_{q=1}^{N_{\text{par}}} \mathrm{Pr}_q p_q(\boldsymbol{u}, t) \end{aligned} \tag{6a}$$

$$p_q(\boldsymbol{u},t)=\frac{1}{\mathrm{Vol}_q}\int_{\Omega_q}\boldsymbol{\delta}[\boldsymbol{u}-\boldsymbol{U}(\boldsymbol{\theta},t)]\mathrm{d}\boldsymbol{\theta} \quad (6b)$$

where $\mathrm{Pr}_q, \mathrm{Vol}_q$ represent the probability measure and the volume measure of Ω_q, respectively.

A set of uniformly distributed densified points $\mathcal{P}_{\mathrm{den}} = \{\tilde{\boldsymbol{\theta}}_l\}_{l=1}^{N_{\mathrm{den}}}$ satisfying $\mathcal{P}_{\mathrm{par}} \subseteq \mathcal{P}_{\mathrm{den}}$ is generated over $\Omega_{\boldsymbol{\Theta}}$. Let n_q denote the number of densified points in each cell Ω_q. Based on the Dirac sequence method Fan et al. (2009), the integral of $\boldsymbol{\delta}(\bullet)$ in Eq. (6b) can be approximated by the Dirac sequence smoothing technique. A parametric kernel function $k_\varepsilon : \Omega_{\boldsymbol{U}} \times \Omega_{\boldsymbol{U}} \to \mathbb{R}$ is adopted, satisfying the following conditions:

$$\int_{\Omega_{\boldsymbol{U}}} k_\varepsilon(\boldsymbol{x},\boldsymbol{y})\mathrm{d}\boldsymbol{y}=1, \forall \boldsymbol{x}\in\Omega_{\boldsymbol{U}} \quad (7a)$$

$$\lim_{\varepsilon\to 0} k_\varepsilon(\boldsymbol{x},\boldsymbol{y})=\boldsymbol{\delta}(\boldsymbol{x}-\boldsymbol{y}), \forall \boldsymbol{x},\boldsymbol{y}\in\Omega_{\boldsymbol{U}} \quad (7b)$$

A common adopted k_ε is the Gaussian kernel. The following approximation holds:

$$p_q(\boldsymbol{u},t)\approx\frac{1}{n_q}\sum_{\tilde{\boldsymbol{\theta}}_l\in\Omega_q} k_\varepsilon[\boldsymbol{u},\boldsymbol{U}(\tilde{\boldsymbol{\theta}}_l,t)] \quad (8)$$

According to KDE theory Botev et al. (2010), the approximation accuracy is given by:

$$\left|p_q(\boldsymbol{u},t)-\frac{1}{n_q}\sum_{\tilde{\boldsymbol{\theta}}_l\in\Omega_q} k_\varepsilon[\boldsymbol{u},\boldsymbol{U}(\tilde{\boldsymbol{\theta}}_l,t)]\right| \le C\left(\frac{1}{\sqrt{n_q}}+\varepsilon^2\right) \quad (9)$$

A set of monitoring points $\{\boldsymbol{u}_i\}_{i=1}^{N_{\mathrm{mon}}}$ is selecеted over $\Omega_{\boldsymbol{U}}$. At each monitoring point $\boldsymbol{u}_i$ and each time instant t_j, Eq. (6a) holds true. A matrix equation can be formulated:

$$\boldsymbol{L}=\boldsymbol{T}\boldsymbol{p} \quad (10)$$

where:

$$[\boldsymbol{p}]_q=\mathrm{Pr}_q \quad (11a)$$

$$\boldsymbol{L}=[\boldsymbol{L}_1^\top,\boldsymbol{L}_2^\top,...,\boldsymbol{L}_{N_t}^\top]^\top \quad (11b)$$

$$[\boldsymbol{L}_j]_i=p_{\boldsymbol{U}}(\boldsymbol{u}_i,t_j) \quad (11c)$$

$$\boldsymbol{T}=[\boldsymbol{T}_1^\top,\boldsymbol{T}_2^\top,...,\boldsymbol{T}_{N_t}^\top]^\top \quad (11d)$$

$$[\boldsymbol{T}_j]_{iq}=p_q(\boldsymbol{u}_i,t_j) \quad (11e)$$

Solving the equation Eq. (10) can be transformed into the corresponding quadratic programming problem within the probability simplex:

$$\underset{\boldsymbol{p}\in\Delta^{N_{\mathrm{par}}}}{\mathrm{argmin}} \quad \boldsymbol{p}^\top\boldsymbol{T}^\top\boldsymbol{T}\boldsymbol{p}-2\boldsymbol{p}^\top\boldsymbol{T}^\top\boldsymbol{L}+\boldsymbol{L}^\top\boldsymbol{L} \quad (12a)$$

$$\Delta^{N_{\mathrm{par}}}=\{\boldsymbol{p}\in\mathbb{R}^{N_{\mathrm{par}}}:\boldsymbol{p}\ge\boldsymbol{0}, \quad \boldsymbol{1}^\top\boldsymbol{p}=1\} \quad (12b)$$

After solving the above optimization problem, the partition point set $\mathcal{P}_{\mathrm{par}}$ is reorganized based on the probability measure vector $\boldsymbol{p}$ to concentrate points in high-probability regions. The problem Eq. (12) is then reformulated and solved iteratively.

To ensure the well-posedness of the problem Eq. (12), the following condition must be satisfied at least:

$$N_t N_{\mathrm{mon}} > N_{\mathrm{par}} \quad (13)$$

Moreover, the dimension $d_{\boldsymbol{\Theta}}$ must match $d_{\boldsymbol{U}}$. If $d_{\boldsymbol{\Theta}} > d_{\boldsymbol{U}}$, no continuous injective mapping exists between $\boldsymbol{\Theta}$ and $\boldsymbol{U}$, so $p_{\boldsymbol{\Theta}}$ cannot be uniquely determined. If $d_{\boldsymbol{\Theta}} < d_{\boldsymbol{U}}$, probability concentrates on a low-dimensional manifold in $\Omega_{\boldsymbol{U}}$, making $p_{\boldsymbol{U}}(\boldsymbol{u},t)$ singular. This is the key shortcoming of the density-based method.

3. The Diffusion Manifold Method (DMM)

To overcome the singularity of the PDF in the high-dimensional space, the diffusion manifold method (DMM) is applied.

Denote $\boldsymbol{X}\in\Omega_{\boldsymbol{X}}=\mathbb{R}^n$ as the response vector, where $\Omega_{\boldsymbol{X}}$ is referred to as the response space. $\boldsymbol{X}$ consists of some components of $\boldsymbol{U}$ at several time instants. Corresponding to the operator equation Eq. (1), the model error and the measurement noise, the following relationship holds:

$$\boldsymbol{X}=\mathcal{M}(\boldsymbol{\Theta})+\boldsymbol{\epsilon} \quad (14)$$

where $\mathcal{M}:\Omega_{\boldsymbol{\Theta}}\to\Omega_{\boldsymbol{X}}$ is the forward mapping, assumed to be smooth; $\tilde{\boldsymbol{X}}=\mathcal{M}(\boldsymbol{\Theta})$ is the model prediction; and $\boldsymbol{\epsilon}$ represents the prediction discrepancy.

If the inverse problem is well-posed, the model prediction $\tilde{\boldsymbol{X}} = \mathcal{M}(\boldsymbol{\Theta})$ lies on a low-dimensional Riemannian manifold $M = \mathcal{M}(\Omega_{\boldsymbol{\Theta}})$, where $\mathcal{M}$ becomes an embedding. The probability measure $\Pr_{\tilde{\boldsymbol{X}}}$ of $\tilde{\boldsymbol{X}}$ is supported on M and possesses the manifold density $\tilde{p}_M$.

In practice, observation data $\mathcal{D}_{\boldsymbol{X}} = \{\boldsymbol{x}_i\}_{i=1}^N$ is available, essentially the realizations of $\boldsymbol{X}$. Model errors and measurement noise cause the observed data $\mathcal{D}_{\boldsymbol{X}}$ to scatter near, but not exactly on M. Thus, the probability measure $\Pr_{\boldsymbol{X}}$ possesses a volume density. A virtual diffusion process $\boldsymbol{Y}_s$ is constructed. Its initial distribution matches $\Pr_{\tilde{\boldsymbol{X}}}$ with manifold density $\tilde{p}_M$, and its transient density $p(\boldsymbol{y}, s)$ approximates the volume density of $\Pr_{\boldsymbol{X}}$.

For simplicity, the stochastic differential equation of $\boldsymbol{Y}_s$ is set to:

$$\mathrm{d}\boldsymbol{Y}_s = \mathrm{d}\boldsymbol{W}_s \tag{15}$$

The transition PDF $p(\boldsymbol{y}, s|\boldsymbol{x}, 0)$ of $\boldsymbol{Y}_s$ and its transient PDF $p(\boldsymbol{y}, s)$ can be obtained:

$$p(\boldsymbol{y}, s|\boldsymbol{x}, 0) = \frac{1}{(2\pi s)^{n/2}} \exp\left(-\frac{\|\boldsymbol{y}-\boldsymbol{x}\|^2}{2s}\right) \tag{16a}$$

$$p(\boldsymbol{y}, s) = \int_M p(\boldsymbol{y}, s|\boldsymbol{x}, 0)\tilde{p}_M(\boldsymbol{x})\nu(\mathrm{d}\boldsymbol{x}) \tag{16b}$$

where $\nu(\bullet)$ is the Riemannian volume measure corresponding to the induced metric. The following can be derived based on the principle of preservation of probability:

$$\tilde{p}_M(\boldsymbol{x})\nu(\mathrm{d}\boldsymbol{x})|_{\boldsymbol{x}=\mathcal{M}(\boldsymbol{\theta})} = p_{\boldsymbol{\Theta}}(\boldsymbol{\theta})\mathrm{d}\boldsymbol{\theta} \tag{17}$$

Use $\mathcal{D}_{\boldsymbol{X}}$ to partition $\mathbb{R}^n$ into Voronoi cells $\mathcal{N}_i, i = 1, 2, ..., N$:

$$\mathcal{N}_i = \{\boldsymbol{x} \in \mathcal{N}_{\boldsymbol{X}} : \|\boldsymbol{x}-\boldsymbol{x}_i\| \leq \|\boldsymbol{x}-\boldsymbol{x}_j\|, \forall \boldsymbol{x}_j \in \mathcal{D}_{\boldsymbol{X}}\} \tag{18}$$

where $\mathcal{N}_{\boldsymbol{X}}$ is a region within $\mathbb{R}^n$ and totally contains $M \cup \mathcal{D}_{\boldsymbol{X}}$, satisfying $\Pr_{\boldsymbol{X}}(\mathcal{N}_{\boldsymbol{X}}) \approx 1$ and the following normalization property:

$$\int_{\mathcal{N}_{\boldsymbol{X}}} p[\boldsymbol{y}, s|\mathcal{M}(\boldsymbol{\theta}), 0]\mathrm{d}\boldsymbol{y} \approx 1, \forall \boldsymbol{\theta} \in \Omega_{\boldsymbol{\Theta}} \tag{19}$$

Construct the partition point set $\mathcal{P}_{\text{par}} \subseteq \Omega_{\boldsymbol{\Theta}}$ and partition $\Omega_{\boldsymbol{\Theta}}$ into Voronoi cells Ω_q. Generate the densified point set $\mathcal{P}_{\text{den}}$ satisfying $\mathcal{P}_{\text{par}} \subseteq \mathcal{P}_{\text{den}}$ as aforementioned and count the number n_q of densified points contained in each cell Ω_q. Introduce the following two approximations:

$$\begin{cases} \Pr_{\boldsymbol{X}}(\mathcal{N}_i) \approx 1/N; \\ \int_{\mathcal{N}_i} p[\boldsymbol{y}, s|\mathcal{M}(\tilde{\boldsymbol{\theta}}_l), 0]\mathrm{d}\boldsymbol{y} \\ \quad \propto \exp\left(-\|\boldsymbol{x}_i - \mathcal{M}(\tilde{\boldsymbol{\theta}}_l)\|^2/(2s)\right). \end{cases} \tag{20}$$

It can be derived that:

$$\begin{aligned} \frac{1}{N} &\approx \int_{\mathcal{N}_i}\int_M p(\boldsymbol{y}, s|\boldsymbol{x}, 0)\tilde{p}_M(\boldsymbol{x})\nu(\mathrm{d}\boldsymbol{x})\mathrm{d}\boldsymbol{y} \\ &= \sum_{q=1}^{N_{\text{par}}} \int_{\Omega_q}\int_{\mathcal{N}_i} p[\boldsymbol{y}, s|\mathcal{M}(\boldsymbol{\theta}), 0]p_{\boldsymbol{\Theta}}(\boldsymbol{\theta})\mathrm{d}\boldsymbol{y}\mathrm{d}\boldsymbol{\theta} \\ &\approx \sum_{q=1}^{N_{\text{par}}} \frac{\Pr_q}{\mathrm{Vol}_q}\int_{\Omega_q}\int_{\mathcal{N}_i} p[\boldsymbol{y}, s|\mathcal{M}(\boldsymbol{\theta}), 0]\mathrm{d}\boldsymbol{y}\mathrm{d}\boldsymbol{\theta} \\ &\approx \sum_{q=1}^{N_{\text{par}}} \Pr_q \frac{1}{n_q}\sum_{\tilde{\boldsymbol{\theta}}_l \in \Omega_q}\int_{\mathcal{N}_i} p[\boldsymbol{y}, s|\mathcal{M}(\tilde{\boldsymbol{\theta}}_l), 0]\mathrm{d}\boldsymbol{y} \\ &\approx \sum_{q=1}^{N_{\text{par}}} \left(\frac{1}{n_q}\sum_{\tilde{\boldsymbol{\theta}}_l \in \Omega_q} v_{il}\right)\Pr_q \end{aligned} \tag{21}$$

where:

$$v_{il} = \frac{\exp\left(-\|\boldsymbol{x}_i - \mathcal{M}(\tilde{\boldsymbol{\theta}}_l)\|^2/(2s)\right)}{\sum_{j=1}^N \exp\left(-\|\boldsymbol{x}_j - \mathcal{M}(\tilde{\boldsymbol{\theta}}_l)\|^2/(2s)\right)} \tag{22}$$

Thus, the following matrix equation is derived:

$$\boldsymbol{L} = \boldsymbol{T}\boldsymbol{p} \tag{23}$$

where:

$$[\boldsymbol{p}]_q = \Pr_q \tag{24a}$$

$$\boldsymbol{L} = [1, 1, ..., 1]^\top/N \tag{24b}$$

$$[\boldsymbol{T}]_{iq} = \frac{1}{n_q}\sum_{\tilde{\boldsymbol{\theta}}_l \in \Omega_q} v_{il} \tag{24c}$$

Obviously, this equation shares the same form as Eq. (10), and can be transformed into the quadratic programming problem identical in form to Eq. (12).

4. Ill-posedness

The two aforementioned methods are formulated into a unified quadratic programming framework in Eq. (12a), allowing ill-posed problems to be addressed through a consistent approach. The inverse problem becomes ill-posed when the forward mapping is non-injective, resulting in high column-wise similarity and severe rank deficiency in the transition matrix $\boldsymbol{T}$ in Eq. (12a).

Perform a full SVD on $\boldsymbol{T}$ and obtain:

$$\boldsymbol{T} = \begin{bmatrix} \boldsymbol{U}_1 & \boldsymbol{U}_2 & \boldsymbol{U}_3 \end{bmatrix} \begin{bmatrix} \boldsymbol{S}_1 & \boldsymbol{O} \\ \boldsymbol{O} & \boldsymbol{S}_2 \\ \boldsymbol{O} & \boldsymbol{O} \end{bmatrix} \begin{bmatrix} \boldsymbol{V}_1^\top \\ \boldsymbol{V}_2^\top \end{bmatrix} \tag{25}$$

Here, $\boldsymbol{U}_1, \boldsymbol{S}_1, \boldsymbol{V}_1$ correspond to the r largest singular values, and $\boldsymbol{U}_2, \boldsymbol{S}_2, \boldsymbol{V}_2$ to the remaining $N_{\text{par}} - r$ negligible ones. The following approximation reads:

$$\boldsymbol{T} \approx \boldsymbol{U}_1 \boldsymbol{S}_1 \boldsymbol{V}_1^\top \tag{26}$$

Decomposition the desired probability measure vector $\boldsymbol{p}$ in the following form:

$$\boldsymbol{p} = \boldsymbol{V}\boldsymbol{q} = \boldsymbol{V}_1\boldsymbol{q}_1 + \boldsymbol{V}_2\boldsymbol{q}_2 \tag{27}$$

Based on and Eq. (26), the following modified version of the optimization problem Eq. (12) can be obtained:

$$\begin{aligned} \underset{\boldsymbol{q}_1 \in \mathbb{R}^r}{\text{argmin}} \quad & \boldsymbol{q}_1^\top \boldsymbol{S}_1^2 \boldsymbol{q}_1 - 2\boldsymbol{q}_1^\top \boldsymbol{S}_1 \boldsymbol{U}_1^\top \boldsymbol{L} + \boldsymbol{L}^\top \boldsymbol{L} \\ \text{s.t.} \quad & \boldsymbol{V}_1 \boldsymbol{q}_1 \in \Delta^{N_{\text{par}}} \end{aligned} \tag{28}$$

A quality metric $\mathcal{H}(\boldsymbol{p})$ is introduced as prior information to determine $\boldsymbol{q}_2$, where lower values correspond to more desirable configurations of $\boldsymbol{p}$. Thus, a two-step optimization is formulated after SVD of $\boldsymbol{T}$: first solve Eq. (28) for $\boldsymbol{q}_1$, then solve:

$$\begin{aligned} \underset{\boldsymbol{q}_2 \in \mathbb{R}^{N_{\text{par}}-r}}{\text{argmin}} \quad & \mathcal{H}(\boldsymbol{V}_1\boldsymbol{q}_1 + \boldsymbol{V}_2\boldsymbol{q}_2) \\ \text{s.t.} \quad & \boldsymbol{V}_1\boldsymbol{q}_1 + \boldsymbol{V}_2\boldsymbol{q}_2 \in \Delta^{N_{\text{par}}} \end{aligned} \tag{29}$$

The desired probability measure vector is obtained by $\boldsymbol{p} = \boldsymbol{V}_1\boldsymbol{q}_1 + \boldsymbol{V}_2\boldsymbol{q}_2$.

5. Numerical Example

Consider a 10-story 2-span nonlinear frame structure with the Bouc-Wen interlayer restoring force model:Bouc (1967); Wen (1976):

$$\begin{cases} g(X, \dot{X}) = \alpha K X + (1-\alpha) K Z \\ \dot{Z} = \frac{A\dot{X} - \nu\left(\beta\left|\dot{X} Z^{n-1}\right| Z + \gamma \dot{X} |Z|^n\right)}{\eta} \\ \nu = 1 + d_\nu \varepsilon \\ \eta = 1 + d_\eta \varepsilon \\ \varepsilon = \int_0^t Z \dot{X} \mathrm{d}t \end{cases} \tag{30}$$

where the interlayer restoring force $g(X, \dot{X})$ involves the real inner-story drift X and hysteretic displacement Z. Deterministic parameters are specified as: $m = 1 \times 10^4, h = 4.0, \xi_1 = \xi_2 = 0.05, \alpha = 0.01, \gamma = 10, d_\nu = d_\eta = 200$, with m, h, ξ_1, ξ_2 denoting the mass of each story, the height of each story, the first and the second modal damping ratio. The elastic modulus E and parameters β, A are random variables. Their relationship with the 3-dimensional random source $\boldsymbol{\Theta} = (\Theta_1, \Theta_2, \Theta_3)$ is expressed through the following equations:

$$E = 2 \times 10^4 \text{MPa} + 1 \times 10^4 \text{MPa} \cdot \Theta_1 \tag{31a}$$

$$\beta = 10 + 190 \cdot \Theta_2 \tag{31b}$$

$$A = \Theta_3 \tag{31c}$$

where the 3-dimensional random source follows a Gaussian distribution $\mathcal{N}(\boldsymbol{\mu}, \boldsymbol{\Sigma})$ with distribution parameters of $\boldsymbol{\Theta}$ shown in Table. 1.

Table 1. Values of distribution parameters

Parameters	Values
$\boldsymbol{\mu}$	$(0.5, 0.5, 0.5)$
$\boldsymbol{\Sigma}$	$0.005 \begin{bmatrix} 1 & -0.5 & 0 \\ -0.5 & 0.6 & 0 \\ 0 & 0 & 1 \end{bmatrix}$

First, noisy observational data were generated. A Monte Carlo simulation comprising 5000 realizations was performed on the frame structure. In each realization, 2 stochastic acceleration excitation samples were applied at the bottom. 5% Gaussian white noise is added to the response of each floor to simulate realistic measurement conditions. The recorded noisy 5-th absolute drift time histories under the first excitation are presented in Fig. 1.

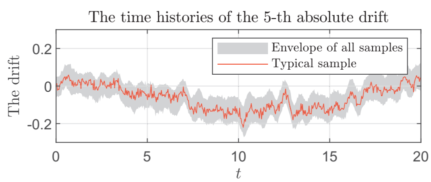

Fig. 1. The sample time histories

Apply the DMM algorithm to identify the probability structure of $\boldsymbol{\Theta}$. The response vector $\boldsymbol{X}$ consists of values of displacements of all stories at 500 uniformly distributed time instants within $[0, 20]$. The identification results are shown in Fig. 2 and Fig. 3. The forward and backward KL-divergences (F-KL, B-KL) between the identified marginal distribution and the ground truth are shown in the Table. 2. The reason for using the KL divergence to measure the quality of the results is that, in the DMM algorithm Zhu and Li (2025a), the partition points themselves concentrate from a uniform distribution to the support of the actual probability measure. Therefore, the KL divergence does not encounter numerical issues related to mismatched support domains. However, since the KL divergence is less sensitive to fine-grained variations in the PDF within the support domain, this approach may overlook discrepancies in the details of the PDF. This is also a limitation of the DMM algorithm, as it directly provides the empirical measure rather than the PDF. Other alternatives, such as moment-based distances or Wasserstein distance, could also be used, but these are not further elaborated upon in this paper.

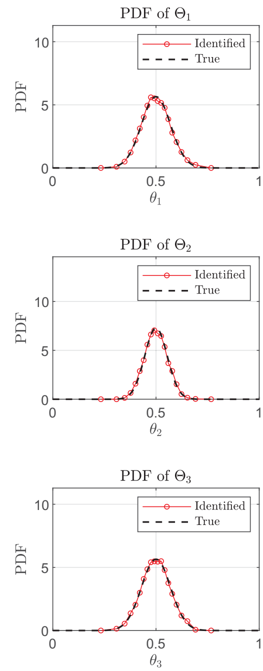

Fig. 2. The identification results of marginal PDFs

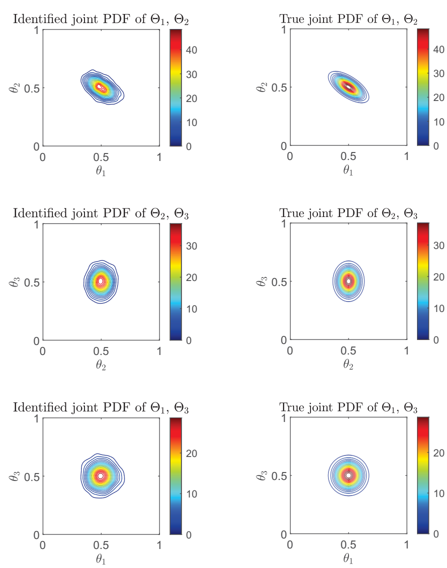

Fig. 3. The identification result of the joint PDFs

Table 2. The forward and backward KL-divergences

Parameters	F-KL	B-KL
Θ_1	0.0036	0.0027
Θ_2	0.0049	0.0049
Θ_3	0.0024	0.0016

6. Conclusion

This study introduces a unified convex optimization framework to infer the probability structure of an unobservable random source from system responses. Two methods are developed: one using response PDFs, and a Diffusion Manifold Method for handling high-dimensional, noisy data. The problem's solvability is characterized via singular value decomposition, with a two-step optimization procedure for ill-posed cases. The framework reliably recovers complex probability distributions without strong prior assumptions.

Acknowledgement

This work was supported by the National Natural Science Foundation of China (Grant No. 51538010).

References

Berenfeld, C., P. Rosa, and J. Rousseau (2024). Estimating a density near an unknown manifold: a Bayesian nonparametric approach. The Annals of Statistics 52(5), 2081–2111.

Botev, Z. I., J. F. Grotowski, and D. P. Kroese (2010). Kernel density estimation via diffusion.

Bouc, R. (1967). Forced vibrations of mechanical systems with hysteresis. In Proc. of the Fourth Conference on Nonlinear Oscillations, Prague, 1967.

Cabral, R., D. Bolin, and H. Rue (2024). Fitting latent non-Gaussian models using variational Bayes and Laplace approximations. Journal of the American Statistical Association 119(548), 2983–2995.

Chen, W., Z. Wang, M. Broccardo, and J. Song (2022). Riemannian Manifold Hamiltonian Monte Carlo based subset simulation for reliability analysis in non-Gaussian space. Structural Safety 94, 102134.

Fan, W., J. Chen, and J. Li (2009). Solution of generalized density evolution equation via a family of δ sequences. Computational Mechanics 43, 781–796.

Feydy, J., T. Séjourné, F.-X. Vialard, S.-i. Amari, A. Trouvé, and G. Peyré (2019). Interpolating between optimal transport and mmd using Sinkhorn divergences. In The 22nd international conference on artificial intelligence and statistics, pp. 2681–2690. PMLR.

Gelfand, A. E. and A. F. Smith (1990). Sampling-based approaches to calculating marginal densities. Journal of the American statistical association 85(410), 398–409.

Geman, S. and D. Geman (1984). Stochastic relaxation, Gibbs distributions, and the Bayesian restoration of images. IEEE Transactions on pattern analysis and machine intelligence (6), 721–741.

Li, J. and J. Chen (2008). The principle of preservation of probability and the generalized density evolution equation. Structural Safety 30(1), 65–77.

Liese, F. and I. Vajda (2006). On divergences and informations in statistics and information theory. IEEE Transactions on Information Theory 52(10), 4394–4412.

Lye, A., A. Cicirello, and E. Patelli (2022). An efficient and robust sampler for Bayesian inference: Transitional ensemble Markov Chain Monte Carlo. Mechanical Systems and Signal Processing 167, 108471.

Mo, J. and W.-J. Yan (2025). Explainable neural-networked variational inference: A new and fast paradigm with automatic differentiation for high-dimensional bayesian inverse problems. Reliability Engineering & System Safety 264, 111337.

Nagel, J. B. and B. Sudret (2016). Hamiltonian Monte Carlo and borrowing strength in hierarchical inverse problems. ASCE-ASME Journal of Risk and Uncertainty in Engineering Systems, Part A: Civil Engineering 2(3), B4015008.

Peyré, G., M. Cuturi, et al. (2019). Computational optimal transport: With applications to data science. Foundations and Trends® in Machine Learning 11(5-6), 355–607.

Wen, Y.-K. (1976). Method for random vibration of hysteretic systems. Journal of the Engineering Mechanics Division 102(2), 249–263.

Wu, Y.-X., D.-C. Feng, and S.-Z. Chen (2025). A refined TMCMC algorithm for adaptive model updating for the probabilistic analysis of complex engineering structures. Structural Safety, 102582.

Ye, N., F. Roosta-Khorasani, and T. Cui (2019). Optimization methods for inverse problems. In

J. de Gier, C. E. Praeger, and T. Tao (Eds.), 2017 MATRIX Annals, pp. 121–140. Springer.

Zhu, Y. and J. Li (2025a). The diffusion manifold method for probabilistic inverse problems. Reliability Engineering & System Safety, 111513.

Zhu, Y. and J. Li (2025b). The probabilistic inverse problem and its solving method based on probability density evolution theory and convex optimization algorithms. Structural Safety 115, 102600.